Nanostructures

International Edition: DOI: 10.1002/anie.201808826
German Edition: DOI: 10.1002/ange.201808826

Direct Synthesis and Pseudomorphic Transformation of Mixed Metal Oxide Nanostructures with Non-Close-Packed Hollow Sphere Arrays

Zhendong Liu, Wenyang Zhao, Prashant Kumar, Xinyu Li, Yasser Al Wahedi, K. Andre Mkhoyan, Michael Tsapatsis, and Andreas Stein**

Abstract: *While bottom-up syntheses of ordered nanostructured materials at colloidal length scales have been successful at producing close-packed materials, it is more challenging to synthesize non-close-packed (ncp) structures. Here, a metal oxide nanostructure with ncp hollow sphere arrays was synthesized by combining a polymeric colloidal crystal template (CCT) with a Pechini precursor. The CCT provided defined confinement through its tetrahedral (T_d) and octahedral (O_h) voids where the three-dimensionally (3D) ordered, ncp hollow sphere arrays formed as a result of a crystallization-induced rearrangement. This nanostructure, consisting of alternating, interconnected large and small hollow spheres, is distinct from the inverse opal structures typically generated from these CCTs. The morphology of the ncp hollow sphere arrays was retained in pseudomorphic transformations involving sulfidation and reoxidation cycling despite the segregation of zinc during these steps.*

Macroscopic properties and application-specific performance of nanostructured materials are governed by their compositional heterogeneities and structural features at the nanoscale.[1–3] To tune such features, various synthesis routes, such as templating,[4] chemical vapor deposition,[5] the Kirkendall effect,[6] galvanic replacement reactions,[7] selective leaching,[8] disassembly and self-reassembly,[9] have been developed. Due to the large surface-to-volume ratios of nanostructured materials, manipulating the interfaces involved in the synthesis is crucial to rationally design the nanostructures and tailor their properties.[10] In spite of many efforts in this direction, it remains challenging to precisely control morphology and composition on multiple length scales.

[*] Dr. Z. Liu, P. Kumar, X. Li, Prof. K. A. Mkhoyan, Prof. M. Tsapatsis
Chemical Engineering and Materials Science
University of Minnesota
Minneapolis, MN 55455 (USA)
E-mail: tsapa001@umn.edu
Dr. Z. Liu, W. Zhao, Prof. A. Stein
Department of Chemistry, University of Minnesota
Minneapolis, MN 55455 (USA)
E-mail: a-stein@umn.edu
Prof. Y. Al Wahedi
Department of Chemical Engineering, Khalifa University of Science and Technology, Sas Al Nakhl Campus, P.O. Box 2533, Abu Dhabi (United Arabian Emirates)
Supporting information and the ORCID identification number(s) for the author(s) of this article can be found under https://doi.org/10.1002/anie.201808826.

One approach to manipulate the morphology of nanostructured materials is through templating methods, including templating with colloidal crystals.[11] With close-packed CCTs[12] as molds one typically expects to produce the inverted structure of the original template, keeping the overall periodic features. For example, with face-centered cubic (fcc) assemblies of colloidal spheres, the templated structure is a solid skeleton that surrounds fcc arrays of spheroidal voids, i.e., an inverse opal. While the assembly of colloidal systems is a flexible route to prepare close-packed nanostructures,[13] such a method is lacking for their ncp counterparts.

Ncp hollow sphere arrays are desirable, for example, in photonic crystal applications for devices including optical switches, all-optical chips, and light emitting diodes.[14] A photonic crystal consisting of hollow spheres located at fcc lattice sites and connected to nearest neighbors by cylindrical rods can, with a sufficiently high refractive index gradient, produce multiple large photonic band gaps that are wider than in the case of analogous close-packed photonic crystals.[15] The dielectric contrast needed for band gap formation is lower in the ncp structure than in related close packed photonic crystals.[16] Hollow sphere arrays are also attractive because of their large fraction of void spaces where functional molecules can be loaded and released.[17] Such open structures provide good access to relatively large surfaces, making them interesting for reactive applications, including sorption and catalysis.

Fabrication of ncp nanoshells with hollow interiors that offer increased accessibility typically relies on the use of ncp templates[18] or tedious manipulation of colloidal crystals with nanofabrication techniques such as etching,[19] soft lithography,[20] pulsed laser irradiation,[21] nanorobot-assisted assembly,[22] and other multi-step procedures.[23,24] However, ncp hollow sphere arrays are not expected by direct templating from a close-packed template. The results presented here are, therefore, surprising as they establish that through control of intermolecular interactions between the surface of a polymeric CCT and precursors for a multicomponent oxide, it is possible to directly template interconnected arrays of ncp hollow spheres.

Here we demonstrate this new method to fabricate 3D ordered, ncp hollow sphere arrays using polymeric CCTs in combination with a Pechini precursor,[25] and applying it to a ZnO-CeO_2-Al_2O_3 ternary system. The ncp nanostructure, which features ordered arrays of alternating, interconnected large and small hollow spheres, is distinct from the inverse opal structures typically generated from colloidal crystals.[11] When subjected to sulfidation and reoxidation processes, the

major component in the ncp hollow sphere array, ZnO, can be sulfidated to ZnS and then oxidized back to ZnO while the unique architecture is retained, demonstrating the robustness of this inorganic nanostructure. This method opens up a new avenue for designing and synthesizing hollow nanostructures with complex architectures and multiple components that are potentially suited for photonic, optoelectronic, biological, and catalytic applications.

The CCT was composed of poly(methyl methacrylate) (PMMA) spheres assembled into fcc arrays (Figure 1 a). Rather than the expected inverse replica of the close-packed template, here a novel nanostructure of hollow sphere arrays resulted from the templating synthesis with a Pechini precursor. The Pechini precursor was prepared from citric acid (CA), ethylene glycol (EG) and nitrate salts with a Zn/Ce/Al ratio of 6/3/1 (see Supporting Information). The SEM and TEM images in Figure 1 b and S1 demonstrate that this structure contains ncp arrays of large and small spheres, which are periodically arranged and interconnected to form empty spaces. Figure 1 d shows a high-angle-annular dark-field scanning-TEM (HAADF-STEM) image, which reveals hollow features of the alternating, interconnected large and small spheres with outer diameters of ≈120 nm and 40 nm, respectively (Figure S1). The higher resolution HAADF-STEM images in Figure 1 e,f show that the spheres consist of nanocrystallites with small grain sizes. The Brunauer-Emmett-Teller (BET) surface areas of the ncp hollow sphere arrays, calculated from Ar sorption data, are 53–86 $m^2 g^{-1}$, depending on the size of templating PMMA spheres used. The shapes of the adsorption isotherms change as the voids in the hollow sphere arrays cross the boundary from mesopores to macropores (> 50 nm, see Figure S2). That the ncp hollow sphere arrays are uniform over a long range is further demonstrated by the low magnification SEM images in Figure S3.

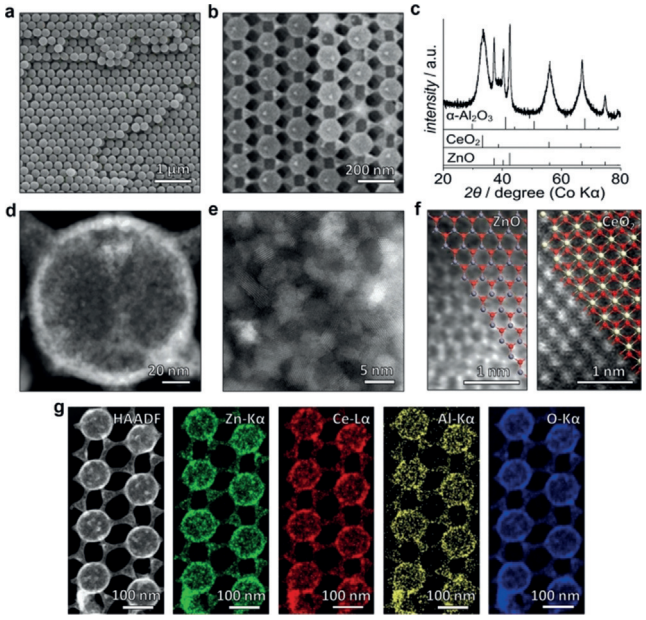

Figure 1. Characterization of the ncp hollow sphere arrays: a) SEM image of the polymeric CCT. b) SEM image of the hollow sphere arrays. c) XRD pattern of the hollow sphere arrays and standard line patterns for ZnO, CeO_2, and α-Al_2O_3. d) HAADF-STEM image of a single hollow sphere, and e) atomic resolution image from the center of the hollow sphere in d showing the individual crystalline grains. f) Atomic resolution HAADF-STEM images with the corresponding crystal structures overlaid for ZnO and CeO_2. g) HAADF-STEM image and corresponding STEM-EDX elemental maps of the hollow sphere arrays. The hollow sphere arrays were synthesized from a Pechini precursor with a Zn/Ce/Al ratio of 6/3/1 using CCTs with 243 nm diameter PMMA spheres.

The crystalline components of the hollow sphere arrays consist mainly of zinc oxide and cerium oxide (Figure 1 c). No peaks from the minor aluminum oxide component are observed in the XRD pattern. The HAADF-STEM image and corresponding STEM-EDX elemental maps in Figure 1 g illustrate that the three components are relatively uniformly distributed in the large and small hollow spheres and connecting bridges. From a typical set of HAADF-STEM images of a single sphere of the hollow sphere arrays (Figure S4), the fractions of Zn, Ce and Al are 27.4 %, 13.7 % and 2.7 %, respectively, comparable to the theoretical metal ratio in the precursor (Zn/Ce/Al = 6/3/1).

The Pechini precursor is one of the key factors that dictate the morphology of the synthesized nanostructures. Tuning of this precursor can alter the intermolecular interactions with the surface of the CCT and consequently generate nanostructures with different morphological features. In particular, ethylene glycol plays an essential role in obtaining the hollow sphere arrays (Figure S5). A composition appropriate for synthesizing the hollow sphere arrays required an EG/CA/metal ratio of 4/2/1. Reducing the EG content by adjusting the EG/CA/metal ratio to 2/2/1 gave a product with the inverse opal structure. In addition, the surface of the CCT matters. Under otherwise identical conditions, we failed to obtain the ncp hollow sphere arrays with PMMA spheres having a negative surface charge. Focusing on CCTs with a positively charged surface, other morphologies such as cube arrays and disassembled hollow spheres could be generated if the Zn/Ce/Al ratio in the Pechini precursor was tuned (Figure S6 and S7).

To understand how the hollow sphere arrays developed, we characterized the products formed at various stages of the synthesis. After the Pechini precursor was infiltrated into the CCT and heated at 90 °C, a metal-containing polymer network was formed as a result of the polyesterification between CA and EG and enveloped the CCT (Figure 2 a). Due to the favorable intermolecular interactions between the precursor and the CCT surface, the deposited oxide tended to closely trace the contours of the PMMA spheres and form a conformal coating over the surface of the CCT.[26] Calcination at 310 °C removed most of the CCT and the polyester components of the Pechini mixture (Figure S8), resulting in a skeleton of the inverse replica of the template (Figure 2 b). A TEM image (Figure 2 d) reveals that the product at this stage consisted of alternating large cubes and small tetrapods with concave surfaces (see also Figure S9). The concave, smooth surfaces of the intermediate material obtained by calcination at 310 °C indicate that it is composed of homogeneous, amorphous nanoparticles. This result is consistent with the

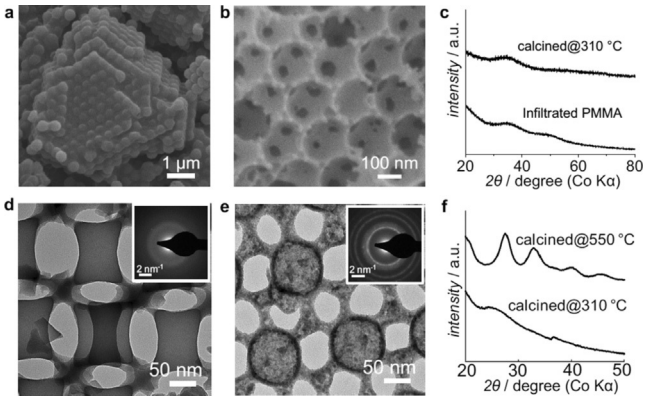

Figure 2. Characterization of products at different stages of the synthesis: a) SEM image of the CCT with the Pechini precursor infiltrated and heated at 90 °C for 24 h. b) SEM image of the sample calcined at 310 °C for 6 h. c) XRD patterns of the infiltrated CCT and the product after calcination at 310 °C for 6 h. d) TEM image and the SAED pattern of the sample after calcination at 310 °C for 6 h. e) TEM image and the SAED pattern of the hollow sphere arrays obtained after calcination at 310 °C followed by further calcination at 550 °C for 2 h. f) Line scan plots of the radially averaged SAED patterns confirm the crystallinity of the hollow sphere arrays upon calcination at 550 °C.

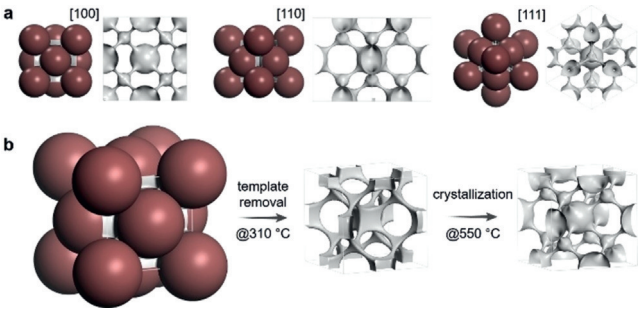

Figure 3. Schematic illustration of the structure and formation of the 3D ordered, ncp hollow sphere arrays: a) The relationship between the CCT and the final hollow sphere arrays viewed along three zone axes of the CCT. Each of the three pairs depicts on the left the final ncp hollow sphere array (grey) embedded in the template (red) and on the right the final array from which the CCT is removed. b) Proposed formation sequence. The empty space of the CCT is filled by amorphous oxide (left) and an inverse opal structure is obtained upon removal of the template (middle). Upon crystallization the inverse opal oxide is transformed to a ncp hollow sphere array (right).

amorphous nature of the material revealed by the XRD pattern (Figure 2c) and the selected area electron diffraction (SAED) pattern (Figure 2d inset). Because of its low crystallinity, the concave surfaces, and associated sharp corners, the material produced by calcination at 310 °C was not stable against further sintering at higher temperatures, and calcination at 550 °C led to the crystalline hollow sphere arrays (Figure 2e and Figure 1). The evolution from the concave cubes to the ballooned hollow spheres occurred concurrently with the crystallization of the metal oxides as demonstrated by peaks in radially averaged SAED patterns (Figure 2f). This suggests that nucleation at the periphery of the cubes and high mobility of the amorphous species are likely key factors enabling this transformation.[27]

The hollow sphere arrays were not generated as residual shells of the templating polymer spheres, but rather in the interstitial spaces of the CCT. The large hollow spheres ($\approx$ 120 nm) are much smaller than the PMMA spheres (243 nm), and the size difference is even greater for the smaller hollow spheres, making it unlikely that they were derived from shrunk shells of PMMA spheres. Moreover, it would be difficult to explain the connectivity of the hollow sphere arrays if they were formed simply by removal of the PMMA spheres, as the geometry of the ncp hollow spheres arrays differs from that of the densely packed CCT. Figure 3a shows the relationship between the CCT and the hollow sphere arrays and illustrates that the geometry of the large and small hollow spheres matches that of the O_h and T_d voids in the fcc colloidal crystal. The sizes of the hollow sphere arrays could be tuned by the size of the PMMA spheres in the CCT. Hollow sphere arrays with larger sizes ($\approx$160 nm and 60 nm for the hollow spheres generated in the O_h and T_d voids) were prepared with PMMA spheres with an average diameter of $\approx$435 nm (Figure S10). Because the periodicity of the hollow sphere arrays originates from the CCT, any specific features of the template, including defects, could also be inherited (Figure S3), implying that ncp hollow sphere arrays of different connectivity should be possible if a template with another symmetry were employed.

Based on the above discussion, the microstructural evolution sequence leading to the formation of this novel hierarchical nanostructure is illustrated in Figure 3b. The CCT provides confinement through its T_d and O_h voids which are infiltrated with the metal-containing precursor. When the CCT is removed by calcination at 310 °C, an amorphous skeleton consisting of interconnected cubes with concave surfaces is generated, with a morphology typically associated with surface templating.[11a] Open windows, originating from contact between adjacent PMMA spheres, become enlarged due to the densification of the metal-containing precursor. Upon further calcination at 550 °C, crystallization-induced rearrangements transform the interconnected, concave cubes into ballooned spheres of the same connectivity, leading to the formation of the ncp hollow sphere arrays.

Ncp hollow sphere arrays with well-defined morphology and specific placement of component species open up a new perspective for applications in catalysis, adsorption, optical and electrochemical devices, and as precursors to other nanostructures.[28] Engineering the compositional heterogeneities and morphological features at the nanometer length scales can improve, for example, the optoelectronic properties.[29] Although the ncp hollow sphere structure obtained here is desirable for photonic crystals,[15] the refractive index contrast obtained with these oxides is too low to expect photonic band gaps. We therefore did not pursue a photonic application here. Instead we employed these materials as sorbents for H_2S removal from low sulfur gas streams and observed interesting pseudomorphic transformations.

To showcase the robustness of the produced nanostructure against chemical transformations, we exposed it to H_2S to transform the ZnO component to ZnS. This was followed by oxygen treatment to convert ZnS back to ZnO. The SEM and TEM images in Figures 4a–c and S11 demonstrate that the

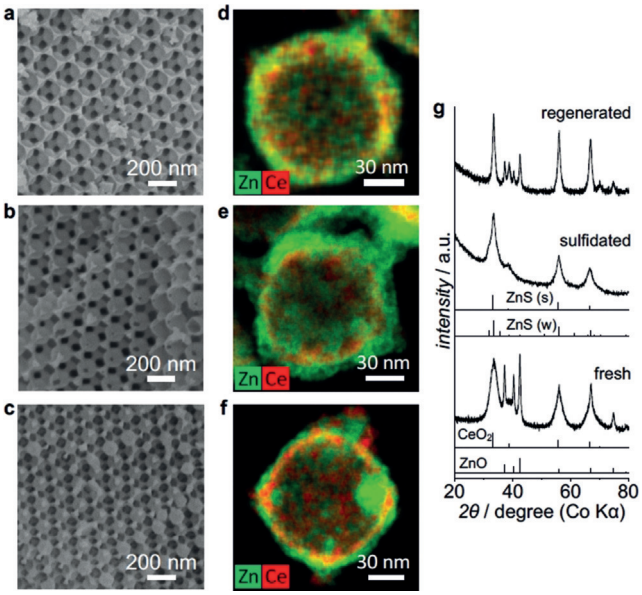

Figure 4. Morphology and microstructure evolution of the hollow sphere arrays during sulfidation and regeneration: a–c) SEM images of the hollow sphere arrays before sulfidation, after sulfidation, and after regeneration, respectively. d–f) STEM-EDX elemental maps showing the locations of Zn and Ce in a single hollow sphere before sulfidation, after sulfidation and after regeneration, respectively. g) XRD patterns of fresh, sulfidated, and regenerated hollow sphere arrays.

overall morphology of the hollow sphere arrays was maintained after sulfidation and even after oxidation despite changes in the elemental distribution and texture. The elemental maps in Figure 4d,f show a comparison of the locations of Zn and Ce inside a single hollow sphere. Initially, all elements were uniformly distributed (Figure 1g and Figure 4d), but after sulfidation, the components became segregated. Zn moved outward after sulfidation, forming an outermost layer that encompassed the Ce species. During sulfidation, it is possible that outward diffusion of Zn was faster compared with inward diffusion of S, resulting in an enrichment of Zn at the outermost part of the hollow spheres. The XRD patterns obtained from these samples (Figures 4g and S12) indicate that wurtzite ZnS was the primary product after sulfidation. Because CeO_2 has a lower thermodynamic preference for reaction with H_2S than ZnO does,[30] CeO_2 did not participate in the sulfidation. Upon oxidation, the wurtzite ZnS was transformed to ZnO. Qualitative inspection of XRD peak broadening indicates that CeO_2 crystals experienced grain growth while ZnO crystallites became smaller compared to the original oxides before sulfidation. Sintering of micro-sized CeO_2 typically requires a higher temperature,[31] but the initial crystallites here are small (<10 nm) and the presence of a transition metal may enhance the sintering of CeO_2.[32] After oxidation, CeO_2 is still evenly distributed. In the case of ZnO, the decrease in peak intensities is possibly because of decreased crystallite size or partial loss of crystallinity. As a result of the Kirkendall effect,[33] the zinc species migrated during sulfidation and formed the sulfidated products at the outer layer of the hollow spheres, which may consist of zinc sulfides with small grains. Consequently, the regeneration carried out in an oxidative atmosphere could possibly generate oxide crystals with a size smaller than the initial one. Despite these local rearrangements, the hollow sphere array morphology was retained. The chemical composition and elemental distribution, at the resolution of the STEM-EDX (ca. 1 nm), were identical for different subunits of the ncp hollow sphere arrays even after sulfidation and partial regeneration (Figure S13). The ability to retain overall connectivity, order, and hollow sphere morphology, despite drastic consecutive changes in composition and crystal structure, may enable uses as reactive adsorbents, catalysts and as precursors to other functional nanostructures.

In summary, we present a novel strategy toward a complex, 3D ordered nanostructure featuring ncp hollow sphere arrays and demonstrate its pseudomorphic transformation from an oxide to a partial sulfide composition and back to the oxide, with a redistribution of metal components during the transformation. The synthesis of this unique architecture involved a polymeric colloidal crystal as the single template, which provided defined confinement through its T_d and O_h voids where the 3D ordered, ncp hollow sphere arrays developed through a remarkable crystallization-induced transformation of concave cubes to hollow spheres. This connected structure was retained when the ZnO portion of the hollow sphere arrays was transformed to ZnS and then back to ZnO. These approaches provide new tools for synthesizing nanostructures with complex architecture and composition.

Acknowledgements

This project is financially supported by the Gas Sub-Committee R&D arm of Abu Dhabi National Oil Company, UAE. Part of this work was conducted at the University of Minnesota Characterization Facility, which receives partial support from the NSF through the NNIN program. We thank Prof. R. L. Penn for use of the XRD.

Conflict of interest

The authors declare no conflict of interest.

Keywords: hierarchical structures · hollow sphere arrays · metal oxide · nanostructures · non-close-packed architecture

How to cite: *Angew. Chem. Int. Ed.* **2018**, *57*, 15707–15711
Angew. Chem. **2018**, *130*, 15933–15937

[1] a) K. C. Christoforidis, P. Fornasiero, *ChemCatChem* **2017**, *9*, 1523–1544; b) Y. Yin, D. Talapin, *Chem. Soc. Rev.* **2013**, *42*, 2484–2487.

[2] a) P. Trogadas, V. Ramani, P. Strasser, T. F. Fuller, M. O. Coppens, *Angew. Chem. Int. Ed.* **2016**, *55*, 122–148; *Angew. Chem.* **2016**, *128*, 128–156; b) G. Prieto, H. Tüysüz, N. Duyckaerts, J. Knossalla, G. Wang, F. Schüth, *Chem. Rev.* **2016**, *116*, 14056–14119.

[3] a) M. Cargnello, P. Fornasiero, R. J. Gorte, *ChemPhysChem* **2013**, *14*, 3869 – 3877; b) Y. Xia, X. Xia, H.-C. Peng, *J. Am. Chem. Soc.* **2015**, *137*, 7947 – 7966.
[4] a) F. Caruso, R. A. Caruso, H. Möhwald, *Science* **1998**, *282*, 1111 – 1114; b) N. D. Petkovich, A. Stein, *Chem. Soc. Rev.* **2013**, *42*, 3721 – 3739; c) H. Blas, M. Save, P. Pasetto, C. Boissiere, C. Sanchez, B. Charleux, *Langmuir* **2008**, *24*, 13132 – 13137; d) B. P. Bastakoti, Y. Q. Li, T. Kimura, Y. Yamauchi, *Small* **2015**, *11*, 1992 – 2002.
[5] Y. D. Xia, Z. X. Yang, R. Mokaya, *Chem. Mater.* **2006**, *18*, 140 – 148.
[6] a) Y. Yin, R. M. Rioux, C. K. Erdonmez, S. Hughes, G. A. Somorjai, A. P. Alivisatos, *Science* **2004**, *304*, 711 – 714; b) H. J. Fan, U. Gosele, M. Zacharias, *Small* **2007**, *3*, 1660 – 1671.
[7] a) E. Gonzalez, J. Arbiol, V. F. Puntes, *Science* **2011**, *334*, 1377 – 1380; b) X. H. Xia, Y. Wang, A. Ruditskiy, Y. N. Xia, *Adv. Mater.* **2013**, *25*, 6313 – 6333.
[8] D. Fodor, F. Krumeich, R. Hauert, J. A. van Bokhoven, *Chem. Eur. J.* **2015**, *21*, 6272 – 6277.
[9] a) H. P. M. de Hoog, M. Nallani, N. Tomczak, *Soft Matter* **2012**, *8*, 4552 – 4561; b) D. M. Vriezema, M. Comellas Aragones, J. A. A. W. Elemans, J. J. L. M. Cornelissen, A. E. Rowan, R. J. M. Nolte, *Chem. Rev.* **2005**, *105*, 1445 – 1490; c) F. Li, S. A. Delo, A. Stein, *Angew. Chem. Int. Ed.* **2007**, *46*, 6666 – 6669; *Angew. Chem.* **2007**, *119*, 6786 – 6789.
[10] M. A. Boles, D. Ling, T. Hyeon, D. V. Talapin, *Nat. Mater.* **2016**, *15*, 141 – 153.
[11] a) A. Stein, B. E. Wilson, S. G. Rudisill, *Chem. Soc. Rev.* **2013**, *42*, 2763 – 2803; b) Y. Z. Li, T. Kunitake, S. Fujikawa, *J. Phys. Chem. B* **2006**, *110*, 13000 – 13004; c) Y. Du, L. E. Luna, W. S. Tan, M. F. Rubner, R. E. Cohen, *ACS Nano* **2010**, *4*, 4308 – 4316; d) L. Xu, J. He, *Langmuir* **2012**, *28*, 7512 – 7518; e) L. Wang, S. A. Asher, *Chem. Mater.* **2009**, *21*, 4608 – 4613; f) Y. Xia, Y. Yin, Y. Lu, J. McLellan, *Adv. Funct. Mater.* **2003**, *13*, 907 – 918; g) P. V. Braun, *Chem. Mater.* **2014**, *26*, 277 – 286.
[12] a) H. Míguez, F. Meseguer, C. Lopez, A. Mifsud, J. S. Moya, L. Vazquez, *Langmuir* **1997**, *13*, 6009 – 6011; b) A. Blanco, F. Gallego-Gomez, C. Lopez, *J. Phys. Chem. Lett.* **2013**, *4*, 1136 – 1142.
[13] Y. Xia, B. Gates, Y. Yin, Y. Lu, *Adv. Mater.* **2000**, *12*, 693 – 713.
[14] Z. Cai, Y. J. Liu, E. S. P. Leong, J. Teng, X. Lu, *J. Mater. Chem.* **2012**, *22*, 24668 – 24675.
[15] a) H. B. Chen, Y. L. Cao, Y. Z. Zhu, Y. P. Wang, Y. B. Chi, *Physica B* **2006**, *381*, 289 – 293; b) M. Doosje, B. J. Hoenders, J. Knoester, *J. Opt. Soc. Am. B* **2000**, *17*, 600 – 606.
[16] a) H. B. Chen, Y. Z. Zhu, Y. L. Cao, Y. P. Wang, Y. B. Chi, *Phys. Rev. B* **2005**, *72*, 113113; b) D. P. Gaillot, C. J. Summers, *J. Appl. Phys.* **2006**, *100*, 113118; c) Y. L. Cao, Y. Z. Zhu, Z. H. Li, J. Ding, J. S. Liu, Y. B. Chi, *Phys. Lett. A* **2007**, *369*, 124 – 127.
[17] a) G. Zhang, H. B. Wu, T. Song, U. Paik, X. W. Lou, *Angew. Chem. Int. Ed.* **2014**, *53*, 12590 – 12593; *Angew. Chem.* **2014**, *126*, 12798 – 12801; b) P. M. Arnal, M. Comotti, F. Schuth, *Angew. Chem. Int. Ed.* **2006**, *45*, 8224 – 8227; *Angew. Chem.* **2006**, *118*, 8404 – 8407.
[18] W. Dong, H. Dong, Z. Wang, P. Zhan, Z. Yu, X. Zhao, Y. Zhu, N. Ming, *Adv. Mater.* **2006**, *18*, 755 – 759.
[19] a) R. Fenollosa, F. Meseguer, *Adv. Mater.* **2003**, *15*, 1282 – 1285; b) R. Fenollosa, F. Meseguer, *J. Mater. Chem.* **2005**, *15*, 4577 – 4580.
[20] a) X. Yan, J. Yao, C. Lu, X. Li, J. Zhang, K. Han, B. Yang, *J. Am. Chem. Soc.* **2005**, *127*, 7688 – 7689; b) J. P. Hoogenboom, C. Retif, E. de Bres, M. van de Boer, A. K. van Langen-Suurling, J. Romijn, A. van Blaaderen, *Nano Lett.* **2004**, *4*, 205 – 208.
[21] K. W. Tan, S. A. Saba, H. Arora, M. O. Thompson, U. Wiesner, *ACS Nano* **2011**, *5*, 7960 – 7966.
[22] F. García-Santamaria, H. T. Miyasaki, A. Urquia, M. Ibisate, M. Belmonte, N. Shinya, F. Meseguer, C. Lopez, *Adv. Mater.* **2002**, *14*, 1144 – 1147.
[23] a) E. Graugnard, J. S. King, D. P. Gaillot, C. J. Summers, *Adv. Funct. Mater.* **2006**, *16*, 1187 – 1196; b) L. Wang, Q. Yan, X. S. Zhao, *J. Mater. Chem.* **2006**, *16*, 4598 – 4602.
[24] T. Udayabhaskararao, T. Altantzis, L. Houben, M. Coronado-Puchau, J. Langer, R. Popovitz-Biro, L. M. Liz-Marzán, L. Vuković, P. Král, S. Bals, R. Klajn, *Science* **2017**, *358*, 514 – 518.
[25] a) M. P. Pechini, US Patent 3330 697, **1967**; b) A. E. Danks, S. R. Hall, Z. Schnepp, *Mater. Horiz.* **2016**, *3*, 91 – 112.
[26] S. G. Rudisill, Z. Y. Wang, A. Stein, *Langmuir* **2012**, *28*, 7310 – 7324.
[27] T. Hansen, A. T. Delariva, S. R. Challa, A. K. Datye, *Acc. Chem. Res.* **2013**, *46*, 1720 – 1730.
[28] a) B. Liu, H. C. Zeng, *Small* **2005**, *1*, 566 – 571; b) E. V. Shevchenko, M. Ringler, A. Schwemer, D. V. Talapin, T. A. Klar, A. L. Rogach, J. Feldmann, A. P. Alivisatos, *J. Am. Chem. Soc.* **2008**, *130*, 3274 – 3275.
[29] a) X. S. Fang, T. Y. Zhai, U. K. Gautam, L. Li, L. M. Wu, Y. Bando, D. Golberg, *Prog. Mater. Sci.* **2011**, *56*, 175 – 287; b) X. S. Fang, L. M. Wu, L. Hu, *Adv. Mater.* **2011**, *23*, 585 – 598.
[30] a) X. Meng, W. de Jong, A. H. M. Verkooijen, *Environ. Prog. Sustainable Energy* **2009**, *28*, 360 – 371; b) M. Husmann, C. Hochenauer, X. Meng, W. de Jong, T. Kienberger, *Energy Fuels* **2014**, *28*, 2523 – 2534.
[31] Y.-C. Zhou, M. N. Rahaman, *J. Mater. Res.* **1993**, *8*, 1680 – 1686.
[32] C. Kleinlogel, L. J. Gauckler, *Adv. Mater.* **2001**, *13*, 1081 – 1085.
[33] J. Park, H. Zheng, Y. Jun, A. P. Alivisatos, *J. Am. Chem. Soc.* **2009**, *131*, 13943 – 13945.

Manuscript received: August 1, 2018
Accepted manuscript online: October 18, 2018
Version of record online: November 9, 2018

